Dronninglund water pit thermal energy storage dataset

Sifnaios, Ioannis; Gauthier, Geoffroy; Trier, Daniel; Fan, Jianhua; Jensen, Adam R.

Published in:
Solar Energy

Link to article, DOI:
10.1016/j.solener.2022.12.046

Publication date:
2023

Document Version
Publisher's PDF, also known as Version of record

Solar Energy 251 (2023) 68–76

Contents lists available at ScienceDirect

Solar Energy

journal homepage: www.elsevier.com/locate/solener

Dronninglund water pit thermal energy storage dataset

Ioannis Sifnaios [a,b,*], Geoffroy Gauthier [c], Daniel Trier [c], Jianhua Fan [a,*], Adam R. Jensen [a]

[a] Department of Civil and Mechanical Engineering, Technical University of Denmark, Koppels Allé, Building 404, 2800 Kgs. Lyngby, Denmark
[b] Sino-Danish College (SDC), University of Chinese Academy of Sciences, Beijing, China
[c] PlanEnergi, Nørregade 13, 1165 København K, Denmark

ARTICLE INFO

Keywords
Heat storage
Seasonal storage
Data analysis
Python
PTES

ABSTRACT

Water pit heat storage has been proven a cheap and efficient storage solution for solar district heating systems. The 60,000 m^3 pit storage in Dronninglund represents in many ways the state-of-the-art large-scale heat storage, demonstrating a storage efficiency higher than 90% during its operation. The storage is used for seasonal and short-term heat storage of solar heat generated by a 37,573 m^2 solar collector field and supplies heat directly to the district heating grid or is used during winter as an alternative heat source to a heat pump. This study aims to provide an overview of the available information on the Dronninglund water pit heat storage, including a detailed description of the design, ground conditions, and operating strategy. The used dataset (2014–2020) has been the foundation for most investigations and simulations of pit thermal energy storages. However, due to a lack of public documentation, various studies have used different post-processing methods and assumptions, leading to inconsistent results. Therefore, the dataset has been manually quality-controlled, and erroneous data have been removed with the aim of establishing a high-quality reference dataset. Moreover, an overview of the available parameters and metadata is provided, along with example plots. To promote the usage of the quality-controlled dataset, all the developed quality-control routines and Python scripts are made available on GitHub.

1. Introduction

In Denmark, where 64% of residential consumers use district heating, incorporating large-scale solar heating plants has become increasingly popular after 2010. Due to the seasonal mismatch between solar heat generation and heat demand, typical district heating systems are limited to achieving a solar thermal fraction of up to 20% (Perez-Mora et al., 2018). To cover this mismatch, seasonal heat storage systems have been used to store the produced thermal energy in summer and use it in winter. By incorporating a seasonal heat storage, the solar thermal fraction of a district heating system can increase up to 50% (Sveinbjörnsson et al., 2017). Four main types of thermal energy storages have been utilized so far for seasonal thermal energy storage (TES), namely, tanks (TTES), boreholes (BTES), aquifers (ATES), and pit thermal energy storages (PTES) (Pauschinger et al., 2018).

The main driver for the PTES technology was to develop a low-cost heat storage for solar district heating systems. PTES systems have been demonstrated combined with large-scale collector fields providing a promising storage solution (Soerensen and From, 2011). Due to the simple storage design, it has been possible to achieve costs below 27 €/m^3 (Schmidt et al., 2018).

In principle, a PTES is a large water reservoir lined with a watertight polymer liner (to prevent water from leaking to the ground) and covered with a floating insulating lid (to reduce heat losses). At the moment of writing, there are six operational pit storages in the world, located in Denmark and Tibet, China. The Danish PTES systems are located in Marstal (75,000 m^3) (Jensen, 2014), Vojens (200,000 m^3) (Rambøll, 2015), Toftlund (70,000 m^3) (Rambøll, 2016), Gram (122,000 m^3) (PlanEnergi, 2015a), and Dronninglund (60,000 m^3) (Schmidt and Sørensen, 2018). In Tibet, there is a PTES in Langkazi (15,000 m^3) (Aalborg CSP, 2019). Apart from these storages, there is a 70,000 m^3 PTES under construction in Høje Taastrup, Denmark, and detailed plans have been made for two storages in Odense, Denmark.

The performance of the existing PTES varies, with Gram having an efficiency of 60% (PlanEnergi, 2020), Marstal 66% (Schmidt, 2019), Toftlund 70% (Rambøll, 2020), and Dronninglund greater than 90% (Winterscheid and Schmidt, 2017). The difference in efficiencies is mainly due to different technologies used for the PTES components (especially the lid) but also due to improved PTES construction. It has to be noted that it was not possible to find information on the performance

* Corresponding authors.
E-mail addresses: iosif@dtu.dk (I. Sifnaios), jifa@dtu.dk (J. Fan).

https://doi.org/10.1016/j.solener.2022.12.046
Received 15 November 2022; Received in revised form 14 December 2022; Accepted 27 December 2022
Available online 17 January 2023

Fig. 1. Aerial view of the PTES and solar collector field in Dronninglund.

of the PTES systems in Vojens and Tibet.

The water pit heat storage in Dronninglund (see Fig. 1) represents, in many ways, the state-of-the-art heat storage technology. For this reason, the majority of investigations and simulations of PTES have used this storage as a reference case, e.g., Dahash et al. (2020,2019), Gauthier (2020), Ochs et al. (2020), Sorknæs (2018), Xie et al. (2021), Pan et al. (2022), Sifnaios et al. (2022).

Nonetheless, some reports for the storage in Dronninglund are only available in Danish. This has led some previously published articles (e.g., Dahash et al. (2021) and Dahash et al. (2020)) to report different ground properties and groundwater levels compared to the official measurement reports. In addition, the published studies are generally limited to only using one or two years of data, even though the storage has been in operation for more than seven years.

However, since the spring of 2021, the operation data of the Dronninglund PTES has been obtained from the Danish company PlanEnergi. According to the data license agreement with the plant, data has not been made available online.

The main objective of this article is to summarize the available knowledge on the Dronninglund PTES and give a detailed explanation of its design and operation. The paper also aims to make interested parties aware of the value of a comprehensive dataset and establish a standardized post-processing procedure, to avoid erroneous measurements being used. Additionally, the paper provides users with an overview of available parameters, which have not been published before, and references to existing documentation of the system, along with the available metadata. Finally, it provides code examples of how to use the data. The developed code is publicly available on the GitHub repository https://github.com/PitStorages/DronninglundData, along with the data for the first year of the plant's operation for testing the code.

The present paper provides a description of the Dronninglund PTES, briefly introducing the storage design and construction. Afterward, information about the location and type of measurement sensors is presented, followed by a description of the data quality control procedure and handling of missing data. Last, several example plots using the quality-controlled dataset are presented.

2. Storage description

Dronninglund is a Danish town in Northern Jutland with approximately 1,350 district heating (DH) consumers and an annual heat demand of approximately 40 GWh (12 MW peak load) (Dronninglund Fjernvarme, 2020). The research project SUNSTORE 3 started in 2008, intending to demonstrate seasonal heat storage coupled with a solar thermal collector field and a heat pump. A 60,000 m^3 pit thermal energy storage (PTES), 37,573 m^2 of flat-plate solar collectors, and an absorption heat pump were constructed as part of the project. The solar collectors installed were Arcon 35/10 HEATstore collectors with insulating foil (Epp, 2014). The cost related to the storage was approximately 2.3 million € (38.3 €/m^3), while the total project cost was approximately 14.1 million € (PlanEnergi, 2015b). The project costs are presented in Table 1.

Table 1
Project costs (PlanEnergi, 2015b).

Component	Cost [€]
Solar collectors	5,856,000
Solar field, excavation, and mounting of pipes	321,000
District heating pipes	985,000
Transmission pipe, excavation, and mounting	344,000
Technique building	3,201,000
Storage heat exchangers, pumps, valves, pipes, diffusers	350,000
Storage excavation and landscaping	673,000
Storage lid and liner	1,263,000
Other costs	1,137,000

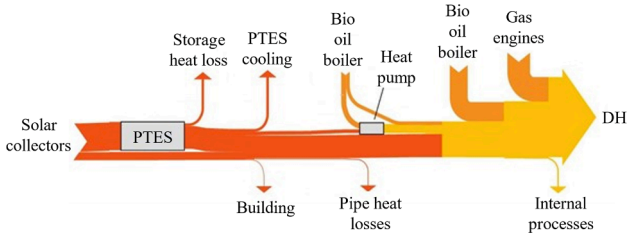

Fig. 2. Schematic of the expected energy flows for the original plant (modified from Winterscheid and Schmidt, 2017).

2.1. Dronninglund heating system

The priority for the solar thermal collectors was to supply heat directly to the district heating grid. If the solar heat production was higher than the demand, the surplus heat was used to charge the PTES. In periods with low or no solar heat production, the storage could supply heat directly to the district heating grid, but only if the outlet temperature was above 75 °C. Net charging of the storage typically occurred from February to August, whereas net discharging occurred from September to January. Depending on the specific year, February, August, and September could either have net charging or discharging (see Fig. 14 for monthly charged/discharged energy).

If the temperature of the PTES was not sufficiently high, the storage was used as the low-temperature heat source for a 5.2 MW absorption heat pump (2.1 MW cooling capacity) with a COP of 1.67. The heat pump was driven by high-temperature heat from a 5 MW bio-oil boiler. The heat pump generally started operating around the start of November and continued until January or February. The inlet temperature of the heat pump's source side was 75 °C or lower (depending on the temperature at the top of the PTES), and it cooled the storage down to approximately 10 °C. The connection of the heat pump to the storage is illustrated in Fig. 3.

The absorption heat pump, the 5 MW bio oil boiler, and an additional 10 MW bio-oil boiler were located at the Søndervang district heating plant in the town, approx. 2.5 km away from the PTES. At a second location in the town, Tidselbak Alle, there was also an 8 MW natural gas boiler and four 1.6 MW natural gas engines. A Sankey diagram of the expected energy flows for the original plant is illustrated in Fig. 2, and a schematic of the plant is shown in Fig. 3.

It should be mentioned that the PTES system in Dronninglund has been significantly modified during 2022. For example, the original lid solution was replaced with a newer, improved design since the original

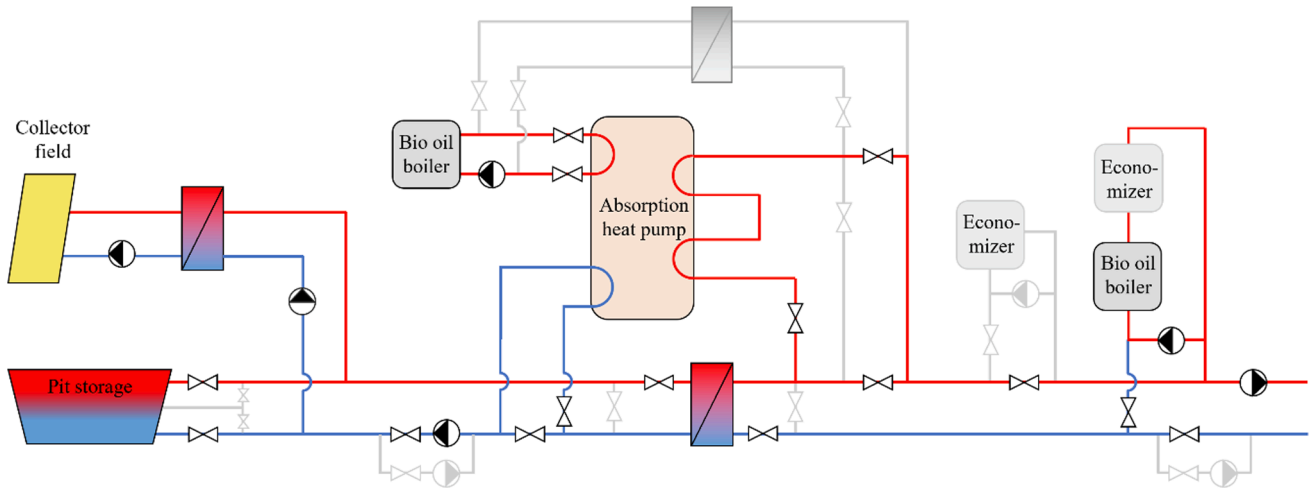

Fig. 3. Simplified schematic of the collector field, the PTES, and the components located in the Søndervang plant (modified from (PlanEnergi, 2015b)).

Fig. 4. Excavation and pipe layout in Dronninglund PTES (PlanEnergi).

Fig. 5. Installation of the bottom liner of the Dronninglund PTES (PlanEnergi).

lid was damaged beyond feasible repair. The damage was caused due to water entering the lid construction through a tear in the bottom lid liner. In addition, the absorption heat pump and bio-oil boiler were replaced by a compression heat pump. However, since the dataset is from 2014 to 2020, the information presented below refers to the original plant configuration.

2.2. Storage design and dimensions

The PTES has the shape of a truncated pyramid with a depth of 16 m and a volume of 60,000 m^3. The bottom of the pit is a square of 26 × 26 m, and the lid surface is approximately 91 × 91 m, corresponding to a surface area of 8,300 m^2. The storage sides have a slope of 1:2 in order to ensure soil stability.

Three pipes are entering the storage from below, as seen in Fig. 4. At the end of each pipe, there is a diffuser for reducing the mixing caused by the inlet jet flow, assisting in establishing a high degree of stratification in the PTES. Each diffuser consists of two parallel discs with a diameter of 2.5 m and vertical spacing of 0.58 m. The three diffusers are placed at different heights from the bottom of the storage: the top diffuser at 15.3 m, the middle diffuser at 10.9 m, and the bottom diffuser at 0.4 m. These heights are measured at the center of the diffuser opening.

2.3. Storage construction

The PTES construction started in March 2013 and was officially completed in April 2014. Different construction stages are illustrated in Figs. 4 and 5. The solar collectors' heat production (and thus the charging of the storage) began in February 2014.

The excavated soil from the pit was used to form embankments around the pit so that soil would not have to be transported off the site, thus minimizing construction costs. The soil excavation was completed after two months.

After the soil excavation and pipe installation, the PTES was lined with a polymer liner to prevent the stored water from leaking into the ground (see Fig. 5). The watertight liner was a 2.5 mm welded high-density polyethylene (HDPE) with a guaranteed lifetime of 20 years when exposed to temperatures lower than 90 °C. The liner installation took one month and was completed by mid-June 2013; afterward, it took two months to fill the storage with water.

The storage was filled with treated water from the district heating grid to avoid corrosion of the metallic components, e.g., the pipes and diffusers. As part of the water treatment, all salts were removed (including chlorides) in addition to ensuring a low hardness (<0.1 °dH), low conductivity (130 µS/cm), low iron (<0.005 mg/l), low oxygen content (<20 µg/L), and a pH value of 9.8 ± 0.2 (Klingaard and Andersen, 2018). The water quality is analyzed at least annually, and a sodium hydroxide solution is added at regular intervals to maintain the pH level.

After the storage was filled with water, the lid construction started. The original lid design was based on flexible insulation mats enclosed within a top and bottom liner. This allowed the lid to move as the water level changed due to the change of water density with temperature.

The lid insulation consisted of three 80 mm thick layers of Nomalén

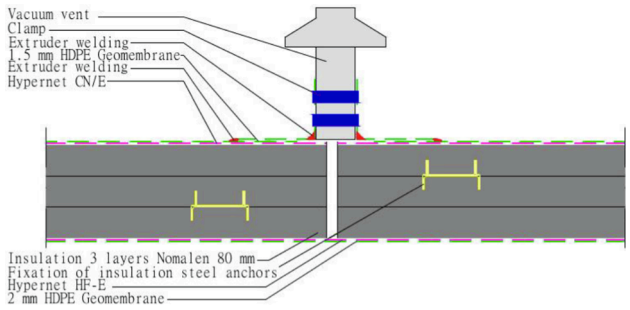

Fig. 6. Sketch of the Dronninglund lid cross-section (PlanEnergi, 2015b).

Table 2
Groundwater properties (GEO, 2012).

Parameter	Value	Unit
Hydraulic conductivity	$3.6 \cdot 10^{-5}$	m/s
Effective porosity	0.25	–
Hydraulic gradient	1/300	–
Groundwater velocity	$4.8 \cdot 10^{-7}$	m/s

Table 3
Thermal properties of soil around storage (GEO, 2010).

	Bulk density [kg/m^3]	Thermal conductivity [W/(m K)]	Specific heat capacity [J/(kg K)]
Above groundwater	1830	0.3–0.5	800
Below groundwater	2040	1	1632

28 N insulation mats manufactured by NMC (NMC Termonova, 2011). Nomalén is made of a closed-cell structure polyethylene (PE) foam with an operating temperature of up to 95 °C. The manufacturer stated that the thermal conductivity of the insulation was 0.04 W/(m K) at 10 °C (NMC Termonova, 2015). Analysis of the operation data showed that the long-term average value of the insulation's thermal conductivity was 0.047 W/(m K) since it was exposed to temperatures up to 90 °C. Nonetheless, it has to be mentioned that the heat flux through the lid was measured at a specific spot in the lid, thus it is not necessarily representative of the heat flux through the entire lid and might underestimate the actual heat flux at times.

Concrete-filled weight pipes were placed inside and on top of the lid. The pipe diameter was increased closer to the center of the lid, creating a slope towards the center. Due to the sloped surface, rainwater was collected at the center of the lid, where it was pumped off the lid's surface. Removal of rainwater is one of the biggest challenges with the PTES lid designs, and inadequate handling of rainwater increases maintenance, heat losses, and shortens the lifetime of the lid.

Additionally, vacuum vents were installed close to the lid's edge to ventilate the interior of the lid construction. Some of the vents were modified in order to allow cold, dry air to be drawn into the lid, where it would absorb heat and moisture. The warm, humid air was vented out by the remaining vents creating natural ventilation. A cross-sectional view of the original lid's construction is shown in Fig. 6.

2.4. Soil and groundwater properties

During the pre-feasibility study, the Danish company GEO was hired to carry out geological investigations, which included measurements of the groundwater level, soil characterization, and estimation of the soil thermal properties. The groundwater level was found to be 1–1.5 m below the bottom of the storage and flowing north to south with an estimated velocity of 15 m/year (GEO, 2012). The same report mentions

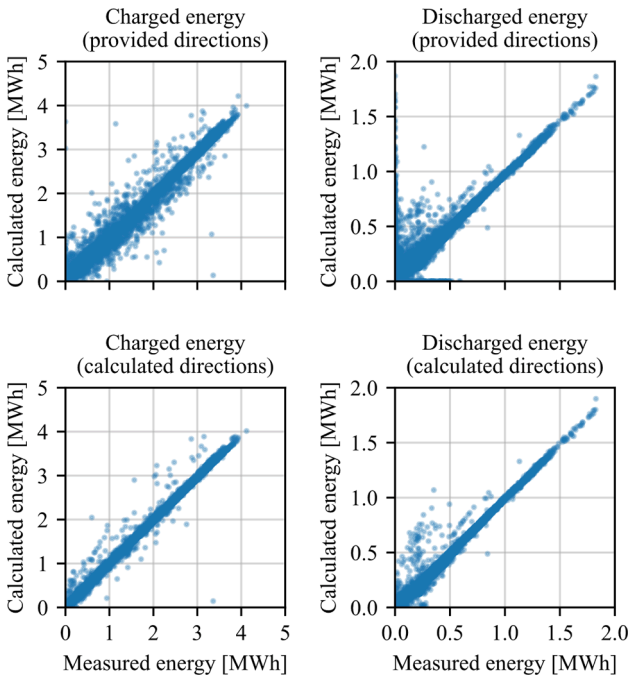

Fig. 7. Calculated charged and discharged energy using the provided and the calculated flow rates, and comparison to the measured energy quantities.

that the groundwater table is not entirely flat (there is a slope of around 1%) and stresses the fact that the depth of groundwater depends on the period of the year, as rainfall, snowmelt, and dry periods can affect it. Nonetheless, in temperate-cold climates (like Denmark), the seasonal level of change for groundwater is below 10% (Nygren et al., 2020). The groundwater properties are presented in Table 2.

Soil investigations revealed that the surrounding soil type is mainly fine sand with a few clay layers (PlanEnergi, 2011). The thermal properties of the soil surrounding the storage were reported by GEO (2010) and are presented in Table 3. According to the report, the soil thermal conductivity was estimated based on theoretical values. The specific heat capacity was not reported and thus has been estimated from the soil type, based on the research from Hamdhan and Clarke (2010).

2.5. Storage flow rates

The PTES is charged by the solar collector field via a heat exchanger. During the PTES charge, water can enter the storage via the top or middle diffuser, depending on its temperature and storage operation. Similarly, water can either be drawn from the middle or top diffuser during discharge.

It has to be mentioned that the magnitude and direction of the storage flows were only measured for the middle diffuser. For the top and bottom diffusers, the flow rates and directions reported in the dataset were calculated by the SCADA control system. However, using the provided data for flows results in a significant mass-flow mismatch of the storage (large imbalance between entering and exiting flows). Therefore, the authors have developed a method for deriving the flow magnitudes and directions based on the energy and mass-flow balance of the storage.

There are three diffusers with each two possible flow directions (in or out), and as a result, there are six unique combinations of flow directions. One of the six combinations could be: flow into the storage through the top and middle diffusers (positive direction) and flow out of the storage through the bottom diffuser (negative direction). For each possible combination of flow directions, the flow and energy balances of the storage were calculated for each time step. The mismatch in the flow and energy balances was then normalized using their standard

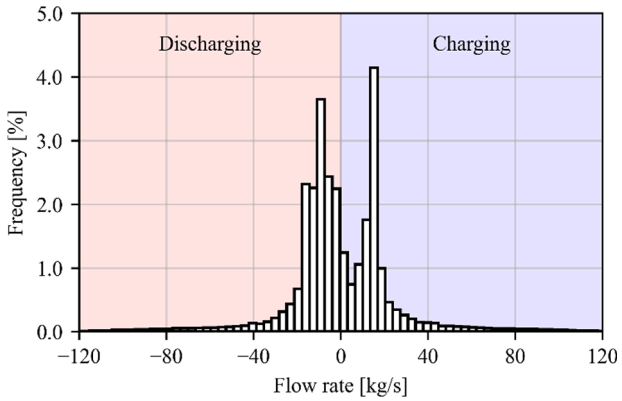

Fig. 8. Histogram with the flow rates used during charging and discharging.

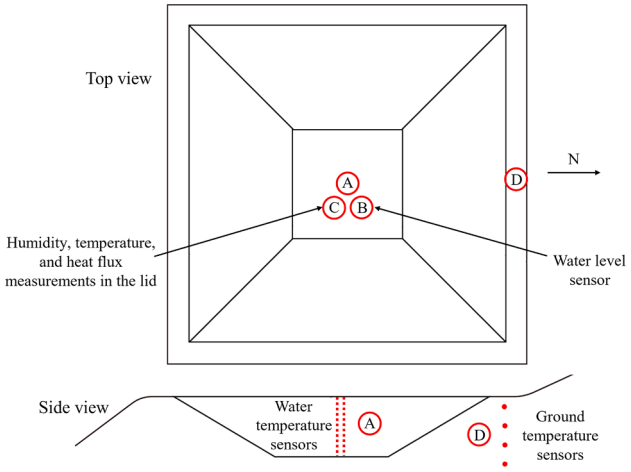

Fig. 9. Measurement locations in and around the Dronninglund pit storage.

deviations for the entire period and added to give a joint "score" for how well each set of directions obeys the flow and energy balance. The set of flow directions that gave the minimum score was then selected for each step.

The calculated flows are in better agreement with the measured charged and discharged energy rates compared to the provided flow directions in the dataset. The exact method for calculating the flow directions is provided in a Python (Python Core Team, 2008) script in the dedicated GitHub repository: https://github.com/PitStorages/DronninglundData.

The energy flows derived from the provided and calculated flow directions are compared in Fig. 7. It can be observed that using the provided flow rate data results in a significant mismatch between the calculated and measured energy. Additionally, mass-flow balance is not achieved when using the provided flow rates. However, mass-flow balance is necessary when using the data as input in simulation models. Thus, the authors recommend using the calculated flow rate magnitudes and directions described in this section.

The frequency distribution of the derived flow rates during charging and discharging is presented in Fig. 8. The mean charge flow rate was 20.2 kg/s, while the mean discharge flow rate was 15.1 kg/s.

It has to be stated that the presented method, though effective, should only be used for the Dronninglund case due to the lack of flow measurements in all diffusers. In the future, it is recommended that the flow magnitude and direction be measured in all diffuser pipes.

3. Measurement sensors

The locations of the sensors in the Dronninglund water pit heat storage are presented in Fig. 9. It has to be noted that although the storage is symmetric, the surrounding ground is very uneven, as can be seen in the side view drawing of Fig. 9; thus, symmetry should not necessarily be assumed for the ground when performing simulations.

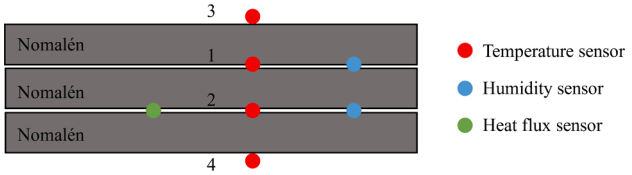

Fig. 10. Placement of temperature sensors in the lid.

3.1. Water temperature measurements

The water temperature is measured with two vertical temperature sensor strings located approximately in the middle of the storage (position A). Each temperature string had 16 temperature sensors placed at 1 m intervals. The two strings are located next to each other and have an offset in their measurement positions of 0.5 m.

3.2. Lid measurements

Initially, a water level sensor was mounted above the top diffuser at position B; however, it operated only from 2015 to 2017 due to the harsh environment. Four temperature and two humidity sensors are installed at position C between the insulation layers, along with a heat flux sensor, as illustrated in Fig. 10. It has to be noted that it is unknown between which two insulation layers the heat flow sensor is placed; however, the specific position should not affect the measurement.

3.3. Ground temperature measurements

Four temperature sensors were installed at position D to measure the ground temperature close to the storage. The exact location of these sensors has not been documented and is thus uncertain. However, according to the plant operator, they are approximately placed in the middle of the storage's northern edge at a 1 m distance from the water edge. The four temperature sensors are located at a depth of 10, 15, 20, and 25 m beneath the top of the embankment.

3.4. Ambient air temperature

The ambient temperature close to the storage is measured in two different locations in the solar collector field in the original dataset. However, the locally measured temperatures are very high (reaching 50 °C during summer). The reason is that the ambient temperature sensors are not properly shielded from direct solar irradiance and that the measurements are probably affected by the emitted heat from the solar collectors.

However, the ambient temperature is also measured by a nearby weather station (06031 Tylstrup) operated by the Danish Meteorological Institute (DMI). The DMI station is approximately 18 km west of the storage, but it is considered representative for long-term studies of the storage heat losses. An added benefit of using DMI's station for the ambient temperature is that the measurements are high quality from ventilated enclosures and are freely available for download from DMI.

3.5. Description of measurement tags

Measurements are made every 10 s and saved every 10 min. The saved values are averaged during the 10-minute periods, except for energy values, which are integrated over the period (MWh). A list of the sensors related to the pit storage is given in Table 4, including the tag name, description, sensor type, unit, and uncertainty for each sensor.

Table 4
List and description of sensors in Dronninglund storage.

Tag name	Description	Sensor Type	Unit	Uncertainty
SO.DA. TT.401.1	Temperature of pit storage bottom layer (0.5 m)	PT100	°C	0.15 K
SO.DA. TT.402.1	Temperature of pit storage at 1 m	PT100	°C	0.15 K
SO.DA. TT.401.2	Temperature of pit storage at 1.5 m	PT100	°C	0.15 K
⋮	⋮	⋮	⋮	⋮
SO.DA. TT.402.15	Temperature of pit storage at 15 m	PT100	°C	0.15 K
SO.DA. TT.401.16	Temperature of pit storage at 15.5 m	PT100	°C	0.15 K
SO.DA. TT.402.16	Temperature of pit storage top layer (16 m)	PT100	°C	0.15 K
SO.DA. HT.422.1.F	Lid humidity at position C point 1	–	%	–
SO.DA. HT.422.1.T	Lid temperature at position C point 1	PT100	°C	0.15 K
SO.DA. HT.422.2.F	Lid humidity at position C point 2	–	%	–
SO.DA. HT.422.2.T	Lid temperature at position C point 2	PT100	°C	0.15 K
SO.DA. TT.422.3	Temperature above lid at position C point 3	PT100	°C	0.15 K
SO.DA. TT.422.4	Temperature below lid at position C point 4	PT100	°C	0.15 K
SO.DA. ET.422.5	Heat flux through lid at position C	Hukseflux HFP01	W/m^2	6–20%
SO.DA. TT.426.1	Ground temperature at 25 m depth	PT100	°C	0.15 K
SO.DA. TT.426.2	Ground temperature at 20 m depth	PT100	°C	0.15 K
SO.DA. TT.426.3	Ground temperature at 15 m depth	PT100	°C	0.15 K
SO.DA. TT.426.4	Ground temperature at 10 m depth	PT100	°C	0.15 K
SO.DA. LT.421	Storage water level measurement	–	m	–
SO.LA. TT.414	Top diffuser temperature	PT100	°C	0.15 K
SO.LA. TT.415	Middle diffuser temperature	PT100	°C	0.15 K
SO.LA. TT.416	Bottom diffuser temperature	PT100	°C	0.15 K
SO.LA.FT.466	Flow rate from the top diffuser	Derived	m^3/hr	–
SO.LA.FT.467	Flow rate from the middle diffuser	Electromagnetic	m^3/hr	0.4 %
SO.LA.FT.468	Flow rate from the bottom diffuser	Derived	m^3/hr	–
SO.LA. FT.466. RETN	Flow direction from the top diffuser[1]	–	–	–
SO.LA. FT.467. RETN	Flow direction from middle diffuser[1]	–	–	–
SO.LA. FT.468. RETN	Flow direction from bottom diffuser[1]	–	–	–
SO.LA. ENERGI. TIL.LAGER. T	The cumulative sum of the charged energy	PT100 + ultrasonic	MWh	0.15–0.5 %
SO.LA. ENERGI. FRA. LAGER.T	The cumulative sum of the discharged energy	PT100 + ultrasonic	MWh	0.15–0.5 %
SO.LA.FT.464	Flow rate to grid/heat pump	Electromagnetic	m^3/hr	0.4 %
SO.LA. TT.411	Supply temperature to grid/heat pump	PT100	°C	0.15 K
SO.LA. TT.410	Return temperature from grid/heat pump	PT100	°C	0.15 K
SO.F.TT.405	Temperature at the north side of the collector field[2]	PT100	°C	0.15 K
SO.F.TT.413	Temperature at the south side of the collector field[2]	PT100	°C	0.15 K
SO.F1.PRO. ENERGI.T	Produced solar energy from field 1	PT100 + ultrasonic	MWh	0.15–0.5 %
SO.F1.AFBL. ENERGI.T	Energy used for storage night cooling field 1	PT100 + ultrasonic	MWh	0.15–0.5 %
SO.F1. FROST. ENERGI.T	Energy used for defrosting field 1 in the winter	PT100 + ultrasonic	MWh	0.15–0.5 %
SO.F2.PRO. ENERGI.T	Produced solar energy from field 2	PT100 + ultrasonic	MWh	0.15–0.5 %
SO.F2.AFBL. ENERGI.T	Energy used for storage night cooling field 2	PT100 + ultrasonic	MWh	0.15–0.5 %
SO.F2. FROST. ENERGI.T	Energy used for defrosting field 2 in the winter	PT100 + ultrasonic	MWh	0.15–0.5 %

[1]The flow directions contained in the original dataset have been found to be erroneously and not maintain flow balance. These flow directions should not be used, and instead be derived from the remaining variables.
[2]The ambient air measurements in the dataset have been found erroneous, probably affected by insufficient shading or by heat emitted from the solar collectors. Since these might be unreliable, data from the Danish Meteorological Institute (DMI) could be used as an alternative.

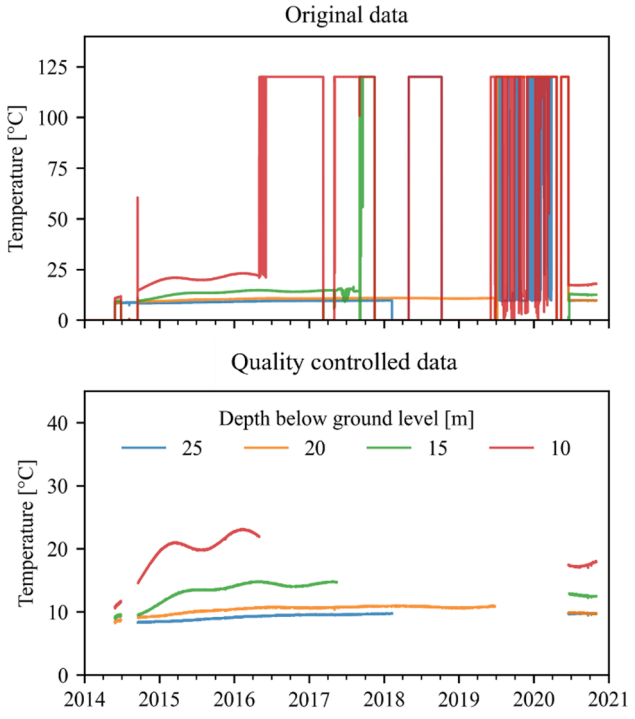

Fig. 11. Soil temperature measurements before and after quality control.

The tag name of each sensor follows a specific structure. The first field is common for all sensors (SO) and represents the solar energy system. The second field describes the subsystem, e.g., DA stands for “damvarmelager” (pit storage) and refers to sensors in or around the storage, LA stands for “lager” (storage) and refers to the sensors located

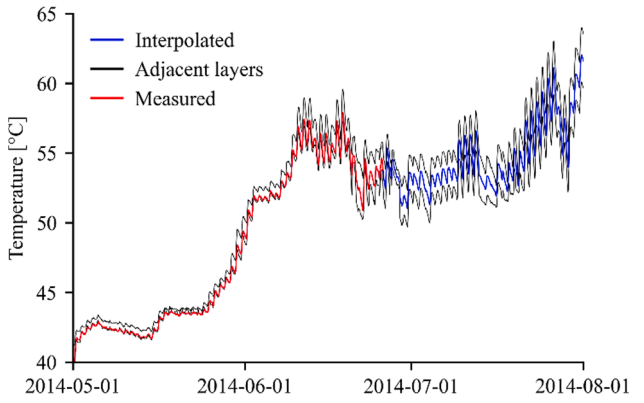

Fig. 12. Measured and interpolated water temperature for the sensor at 1.5 m from the bottom of the storage.

in the pumphouse adjacent to the storage, and F stands for "felt" (field – short form for solar field). The third field is the measured quantity, e.g., TT is temperature, FT is flow, HT is humidity and temperature, ET is heat flux, ENERGI is energy, and LT is water level.

4. Quality control and handling of missing data

The raw measurement data contains many periods with "bad data" due to power outages, sensor failures, etc. These periods have been filtered out using automatic filters and manual inspection. For example, temperatures outside the range 0–100 °C were flagged as erroneous. Afterward, unfeasible temperature spikes were manually removed. The ground temperature data before and after the quality-control procedure is illustrated in Fig. 11.

It has to be noted that all the ground temperature sensors were eventually replaced in the fall of 2021. However, a different position had to be used, approximately 3 m north of the storage's inner edge, as the hole in which the old sensors were installed was closed. Since the new temperature sensors were installed further away from the storage, the measured temperatures are inevitably lower than the previous measurements.

A similar quality control for removing erroneous data was applied to the water temperature measurements. However, in the case of the water temperature sensors, since there were measurements every 0.5 m, the following method was applied in order to reduce the gaps in the data.

Due to the slow time constant of the storage, periods of missing data shorter than 24 h were linearly interpolated. Additionally, missing temperatures were interpolated across the layers. For example, if the temperature at 2.0 m was missing for one month, it was replaced by the average of the sensors at 1.5 m and 2.5 m. This method proved very effective in reducing the number of gaps, as it was infrequent that adjacent temperature sensor data were missing. By interpolating among the layers, most of the long-term gaps were filled. Lastly, we interpolated the missing data for each sensor, filling the remaining gaps and ensuring a complete dataset. Depending on the scope of the analysis, this final step could also be omitted; however, some types of analyses require a complete time series.

As an example, the temperature profile for the sensor at 1.5 m from the storage bottom (SO.DA.TT.401.2) is shown in Fig. 12. The red curve shows the measured temperature, the blue curve is the interpolated temperature based on the sensors above and below, and the black curves are the temperatures of the adjacent layers.

5. Example plots

In this section, example plots are presented to demonstrate the dataset's potential uses. The demonstrated plots aim to provide inspiration to users and only showcase just a small fraction of the available data and possible plots.

Fig. 13 presents the temperature profile in the storage on the first day of each month for 2018. Such figures can be used to inspect the storage temperature profile and the presence of a thermocline layer during different times of the year.

The top subplot of Fig. 14 presents the temperature of the storage layers from 2014 to 2020. The upper layers are illustrated using green color, while the bottom layers are shown in blue. In addition, three thin, black curves are drawn, indicating the temperature of the top, middle, and bottom layers. Such a figure can be used to showcase the seasonally changing temperature profile and identify the years with the highest temperatures in the storage. For example, it is evident that in 2018, the storage had a higher average temperature than in other years, as the temperature of the middle layer was almost equal to the top layer during the charge period. The main reason for this was the increased solar radiation in 2018 compared to an average year.

The middle subplot of Fig. 14 presents the monthly charged and discharged energy as well as the monthly energy content of the storage. When combined with the top subplot, it gives a complete image of the storage operation, e.g., it can be verified that there was more energy charged into the storage in 2018. The middle subplot also demonstrates that the storage was used for both long- and short-term heat storage as a

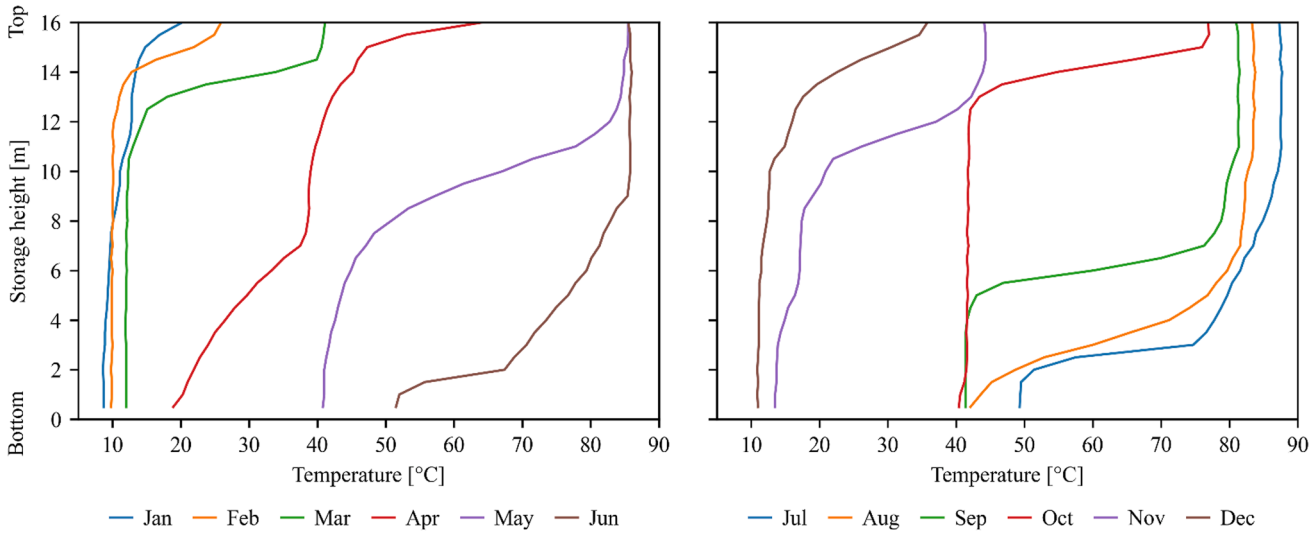

Fig. 13. Temperature profile inside the Dronninglund storage on the 1st day of each month in 2018.

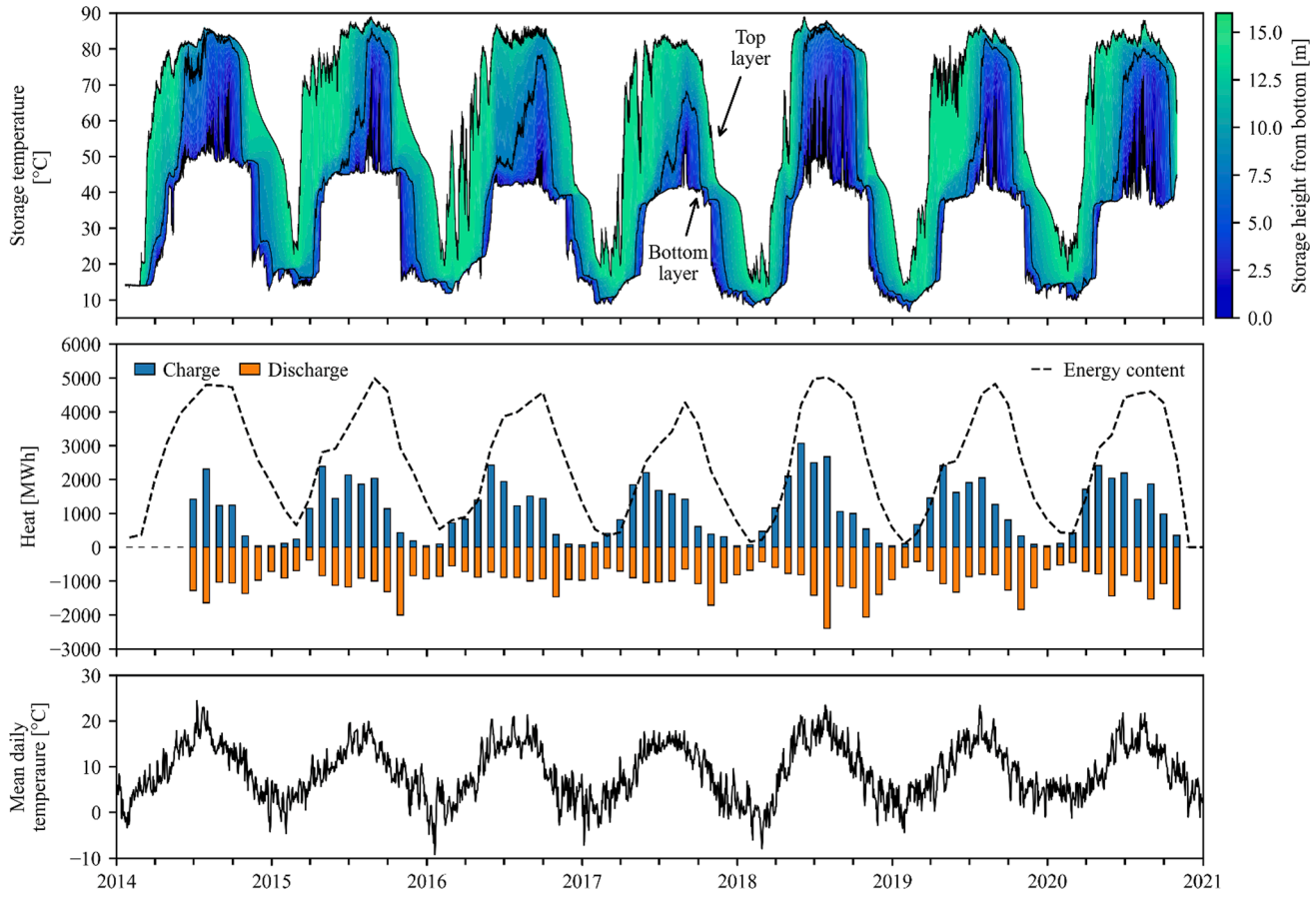

Fig. 14. Dronninglund ambient temperature, storage temperatures, charged and discharged heat, and energy content of the PTES from 2014 to 2020.

significant amount of heat was also discharged in the summer months.

Last, the bottom subplot illustrates the mean daily temperature around the PTEs in Dronninglund, which can be used to identify the yearly high and low ambient temperatures.

5.1. *Moving forward*

This article provides a detailed description of the available information on the Dronninglund water pit heat storage. A reference dataset from the storage operation for the period 2014 – 2020 has been introduced. The goal is for this article to be used as a reference point for future research in the field of seasonal storage of solar thermal heat and specifically for studies regarding the Dronninglund pit storage.

Declaration of Competing Interest

The authors declare that they have no known competing financial interests or personal relationships that could have appeared to influence the work reported in this paper.

Acknowledgments

The authors would like to express their gratitude to Johan Frey for his valuable contributions to the paper. This study was funded by the Danish Energy Agency through EUDP grants' IEA ECES Annex 39 LTES' (no. 64018-0134), 'Participation in the IEA task on efficient solar district heating systems' (no. 134-21027) and 'Participation in the IEA ES TCP Task 41 on Economics of Energy Storage' (no. 134223-495989) and by the Ph.D. program of the Sino-Danish Center for Education and Research (SDC).

References

Aalborg CSP, 2019. 15,000 M3 PTES for district heating, Tibet [WWW Document]. <https://web.archive.org/web/20210418202632/https://www.aalborgcsp.com/projects/15000-m3-ptes-for-district-heating-tibet/> (Accessed 5.4.22).

Dahash, A., Ochs, F., Giuliani, G., Tosatto, A., 2021. Understanding the interaction between groundwater and large-scale underground hot-water tanks and pits. Sustain. Cities Soc. 71, 102928 https://doi.org/10.1016/j.scs.2021.102928.

Dahash, A., Ochs, F., Janetti, M.B., Streicher, W., 2019. Advances in seasonal thermal energy storage for solar district heating applications: a critical review on large-scale hot-water tank and pit thermal energy storage systems. Appl. Energy 239, 296–315. https://doi.org/10.1016/j.apenergy.2019.01.189.

Dahash, A., Ochs, F., Tosatto, A., Streicher, W., 2020. Toward efficient numerical modeling and analysis of large-scale thermal energy storage for renewable district heating. Appl. Energy 279, 115840. https://doi.org/10.1016/j.apenergy.2020.115840.

Dronninglund Fjernvarme, 2020. Dronninglund district heating [WWW Document]. <https://www.dronninglundfjernvarme.dk/>.

Epp, B., 2014. Denmark: Dronninglund Inaugurates 26 MWth Solar District Heating Plant [WWW Document]. Sol. Therm. World. <https://www.solarthermalworld.org/news/denmark-dronninglund-inaugurates-26-mwth-solar-district-heating-plant>.

Gauthier, G., 2020. Benchmarking, and improving models of subsurface heat storage dynamics. Comparison of Danish PTES and BTES installation measurements with their corresponding TRNSYS models. GEOTHERMICA – ERA NET Cofund Geothermal [WWW Document]. <https://www.heatstore.eu/documents/20201028_DK-temadag_PlanEnergi_Monitoring%20results%20for%202019%E2%80%902020%20for%20Marstal,%20Dronninglund%20and%20Gram.pdf>.

GEO, 2012. Dronninglund. Lunderbjerg 8A Damvarmelager - Vurdering af varmelagerets påvirkning af grundvand.

GEO, 2010. Dronninglund. Lunderbjerg 8A Damvarmelager - Geoteknisk undersøgelse.

Hamdhan, I.N., Clarke, B.G., 2010. Determination of Thermal Conductivity of Coarse and Fine Sand Soils, in: Proceedings World Geothermal Congress. Bali, Indonesia.

Jensen, M.V., 2014. Seasonal pit heat storages - Guidelines for materials & construction IEA-SHC Tech Sheet 45.B.3.2.

Klingaard, S., Andersen, A., 2018. Analyse af vandkvalitet og iltindhold i damvarmelageret i Dronninglund.

NMC Termonova, 2015. Thermal properties of Nomalen 28N [WWW Document]. <https://web.archive.org/web/20220428093554/https://dms.etra.fi:9900/72192/conversions/original?version=0> (Accessed 4.28.22).

NMC Termonova, 2011. Nomalen 28N [WWW Document]. <https://web.archive.org/web/20220426161150https://azupcs365certviewer.azurewebsites.net/api/GetSDB?env=se&articleNr=550984> (Accessed 4.20.22).

Nygren, M., Giese, M., Kløve, B., Haaf, E., Rossi, P.M., Barthel, R., 2020. Changes in seasonality of groundwater level fluctuations in a temperate-cold climate transition zone. J. Hydrol. X 8, 100062. https://doi.org/10.1016/j.hydroa.2020.100062.

Ochs, F., Dahash, A., Tosatto, A., Bianchi Janetti, M., 2020. Techno-economic planning and construction of cost-effective large-scale hot water thermal energy storage for Renewable District heating systems. Renew. Energy 150, 1165–1177. https://doi.org/10.1016/j.renene.2019.11.017.

Pan, X., Xiang, Y., Gao, M., Fan, J., Furbo, S., Wang, D., Xu, C., 2022. Long-term thermal performance analysis of a large-scale water pit thermal energy storage. J. Energy Storage 52, 105001. https://doi.org/10.1016/j.est.2022.105001.

Pauschinger, T., Schmidt, T., Alex Soerensen, P., Aart Snijders, D., Djebbar, R., Boulter, R., Jeff Thornton, C., 2018. Integrated Cost-effective Large-scale Thermal Energy Storage for Smart District Heating and Cooling - Design Aspects for Large-Scale Aquifer and Pit Thermal Energy Storage for District Heating and Cooling. Int. Energy Agency Technol. Collab. Program. Dist. Heat. Cool. Incl. Comb. Heat Power, 2018.

Perez-Mora, N., Bava, F., Andersen, M., Bales, C., Lennermo, G., Nielsen, C., Furbo, S., Martínez-Moll, V., 2018. Solar district heating and cooling: a review. Int. J. Energy Res. 42, 1419–1441. https://doi.org/10.1002/er.3888.

PlanEnergi, 2020. Roles in HEATSTORE & Monitoring results for 2019-2020 for Marstal, Dronninglund and Gram [WWW Document]. <https://www.heatstore.eu/documents/20201028_DK-temadag_PlanEnergi_Monitoring%20results%20for%202019%E2%80%902020%20for%20Marstal,%20Dronninglund%20and%20Gram.pdf> (Accessed 12.9.20).

PlanEnergi, 2015a. Long term storage and solar district heating [WWW Document]. <https://web.archive.org/web/20220306155726/https://planenergi.dk/wp-content/uploads/2017/06/sol_til_fjernvarme_brochure_endelig.pdf> (Accessed 5.4.22).

PlanEnergi, 2015b. Sunstore 3 - Phase 2: Implementation.

PlanEnergi, 2011. Sunstore 3, Fase 1 - Projektering og udbud [WWW Document]. <https://energiforskning.dk/sites/energiforskning.dk/files/slutrapporter/slutrapport_incl._bilag_1_12042011_1824.pdf>.

Python Core Team, 2008. Python: A dynamic, open source programming language. Python Software Foundation. <https://www.python.org/>.

Rambøll, 2020. Experience from Toftlund [WWW Document]. <https://www.heatstore.eu/documents/20201028_DK-temadag_Ramb%C3%B8ll%20PTES%20project.pdf> (Accessed 12.9.22).

Rambøll, 2016. Damvarmelagre [WWW Document]. <https://web.archive.org/web/20220504080511/https://dk.ramboll.com/-/media/3fc11649e25942c195fa90e63ea41e11.pdf> (Accessed 5.4.22).

Rambøll, 2015. South-Jutland stores the sun's heat in the world's largest pit heat storage [WWW Document]. <https://web.archive.org/web/20210827074933/https://ramboll.com/projects/re/south-jutland-stores-the-suns-heat-in-the-worlds-largest-pit-heat-storage?utm_source=alias&utm_campaign=sun-storage> (Accessed 5.4.22).

Schmidt, T., 2019. Marstal district heating monitoring data evaluation for the years 2015-2017 [WWW Document]. <https://www.solar-district-heating.eu/wp-content/uploads/2019/10/Marstal-evaluation-report-2015-2017_2019.05.28.pdf> (Accessed 12.9.22).

Schmidt, T., Pauschinger, T., Sørensen, P.A., Snijders, A., Djebbar, R., Boulter, R., Thornton, J., 2018. Design aspects for large-scale pit and aquifer thermal energy storage for district heating and cooling. Energy Proc. 149, 585–594. https://doi.org/10.1016/j.egypro.2018.08.223.

Schmidt, T., Sørensen, P.A., 2018. Monitoring Results from Large Scale Heat storages for District Heating in Denmark.

Sifnaios, I., Jensen, A.R., Furbo, S., Fan, J., 2022. Performance comparison of two water pit thermal energy storage (PTES) systems using energy, exergy, and stratification indicators. J. Energy Storage 52, 104947. https://doi.org/10.1016/j.est.2022.104947.

Soerensen, P.A., From, N., 2011. High solar fraction with pit heat storages, in: 30th ISES Biennial Solar World Congress 2011, SWC 2011. pp. 3020–3030. <https://doi.org/10.18086/swc.2011.21.07>.

Sorknæs, P., 2018. Simulation method for a pit seasonal thermal energy storage system with a heat pump in a district heating system. Energy 152, 533–538. https://doi.org/10.1016/j.energy.2018.03.152.

Sveinbjörnsson, D., Laurberg Jensen, L., Trier, D., Ben Hassine, I., Jobard, X., 2017. Large Storage Systems for DHC Networks.

Winterscheid, C., Schmidt, T., 2017. Dronninglund District Heating Monitoring Data Evaluation for the Years 2015-2017.

Xie, Z., Xiang, Y., Wang, D., Kusyy, O., Kong, W., Furbo, S., Fan, J., 2021. Numerical investigations of long-term thermal performance of a large water pit heat storage. Sol. Energy 224, 808–822. https://doi.org/10.1016/j.solener.2021.06.027.